Applied Surface Science 331 (2015) 50–57

Contents lists available at ScienceDirect

Applied Surface Science

journal homepage: www.elsevier.com/locate/apsusc

The fabrication and photocatalytic performances of flower-like Ag nanoparticles/ZnO nanosheets-assembled microspheres

Quan Deng [a], Haibin Tang [a], Gang Liu [a], Xiaoping Song [b], Guoping Xu [a], Qian Li [c], Dickon H.L. Ng [c], Guozhong Wang [a,*]

[a] Key Laboratory of Materials Physics, Centre for Environmental and Energy Nanomaterials, Anhui Key Laboratory of Nanomaterials and Nanotechnology, Institute of Solid State Physics, Chinese Academy of Sciences, Hefei 230031, P.R. China
[b] Department of Pharmacy, Anhui Medical College, Hefei 230601, P.R. China
[c] Department of Physics, The Chinese University of Hong Kong, Shatin, Hong Kong

ARTICLE INFO

Article history:
Received 5 December 2014
Received in revised form
29 December 2014
Accepted 30 December 2014
Available online 16 January 2015

Keywords:
ZnO
Ag nanoparticle
Microspheres
Micro/nanostructure
Photocatalysis

ABSTRACT

A new micro/nanostructure photocatalyst, Ag nanoparticles decorated ZnO nanosheets-assembled microspheres (Ag-NPs/ZnOs), was synthesised by a two-step method. The flower-like micron-sized ZnO spheres assembled with ~25 nm thick ZnO nanosheets were initially fabricated via a facile solvothermal method. Then, highly dispersed Ag nanoparticles (Ag-NPs) with dimension ranging from 15 to 50 nm were anchored onto the surface of the each ZnO nanosheet by the Sn(II) ion activation method. The as-prepared Ag-NPs/ZnOs demonstrated enhanced photocatalytic performance in eliminating methylene blue and methyl orange aqueous solutions under UV irradiation, showing twice faster reaction rate than the bare ZnOs. The enhanced photocatalytic activity was due to the suppression of electron/hole pair recombination and the acceleration of surface charge transfer induced by the highly dispersive Ag-NPs, which was further demonstrated by the cyclic voltammetry and impedance spectra measurements.
© 2015 Elsevier B.V. All rights reserved.

1. Introduction

It is a pressing need for developing effective and eco-friendly approaches to remove hazardous materials such as dyes, organic compounds, and heavy metallic ions in polluted water. The traditional methods are adsorption, filtration and sedimentation, while recently the improved photocatalysis approaches have gained a great deal of attention owing to its low cost, complete extraction of pollutants, and the formation of harmless by-products [1,2]. In this approach, semiconductor photocatalyst zinc oxide (ZnO) is often being used because it has shown to be a promising agent in environmental remediation [3–7]. However, the efficiency of conventional ZnO photocatalyst is not considerable because of the rapid recombination of the photogenerated electrons and holes of the semiconductor [1,8–10]. Currently, efforts have been placed on the design and modification of the ZnO photocatalyst for achieving large specific surface area, stability, and high segregation effect of electron/hole pairs to achieving high photocatalytic efficiency [11,12].

The nanometer-sized ZnO would provide large specific surface area, supply more active sites on the surface, and thus remarkably increase the photocatalytic efficiency. However, the easy agglomeration of the particles during growth or in the photocatalysis process would result in the reduction of the specific surface area and act against the enhancing effect for photocatalytic performances [10,13]. Therefore, the prevention of agglomeration of the nanometer-sized structure is an important issue for maintaining high photocatalytic activity. In this regard, microstructures assembled with nanostructures (micro/nanostructures) have been proven to have superior structural stability, low agglomeration, easy recovery, and enhanced photocatalytic and adsorption performances [13].

On the other hand, besides the structural design and modification, the decoration of noble metal onto the ZnO is also an effective mean to achieve high photocatalytic activity. The reasons for the enhancement have been proposed as follows: (1) metal particles at the metal-semiconductor interface act as electron sinks which trap the photo-generated electrons and inhibit the recombination of charge carriers [14,15]; (2) specific metal-semiconductor interactions improve the adsorbility of organic pollutant onto the photocatalyst surface [16]; (3) metal particles attract the hydroxyl groups on the semiconductor surface to

* Corresponding author. Tel.: +86 0551 65595616.
E-mail address: gzhwang@issp.ac.cn (G. Wang).

http://dx.doi.org/10.1016/j.apsusc.2014.12.202
0169-4332/© 2015 Elsevier B.V. All rights reserved.

form more active radicals [10]; (4) the introduction of the noble metal changes the concentration of defects in the semiconductor [17,18]. In the previous literatures, Ag/ZnO nanofibers [8], Ag/ZnO hollow microspheres [10], dendrite-like ZnO/Ag heterostructure [19], Ag/ZnO nanoporous microrods [20] have shown significant improved photocatalytic activities in degrading organic contaminants. On the other hand, for the dispersity of metallic Ag in Ag-NPs/ZnO photocatalyst was proven to be a decisive factor to influence the photocatalytic activity [21], it is important to develop another efficient route to obtain high dispersed Ag-NPs on to the surface of different ZnO structures.

Herein, we present a practical and effective method to fabricate a new micro/nanostructural photocatalyst, Ag-nanoparticles decorated ZnO nanosheets-assembled microspheres (Ag-NPs/ZnOs), and the enhanced photocatalytic performances. Firstly, the micron-sized ZnO spheres assembled with ZnO nanosheets were initially synthesised via a facile solvothermal method by controlling the NaOH concentration. Then, highly dispersed Ag-NPs were anchored onto the surface of the each ZnO nanosheet by the Sn(II) ion activation method.The photocatalytic activities and the electrochemical responses of the bare ZnOs and Ag-NPs/ZnOs have been investigated. The results demonstrate that the micro/nanostructural ZnOs modified with high dispersed Ag-NPs have enhanced photocatalysis and improved electrochemical responses, which provide a good candidate material for organic pollutants remediation.

2. Experimental

2.1. Sample fabrication

All chemicals were of analytical grade and used without further purification. $C_4H_6O_4Zn{\cdot}2H_2O$, NaOH, $SnCl_2{\bullet}2H_2O$ and formaldehyde were purchased from Tianjin Guangfu Fine Chemical Research Institute, Shanghai Sinopharm Chemical Reagent Co., Ltd, West Long Chemical Co., Ltd, and Wuxi Zhanwang Chemical Co., Ltd, China, respectively. Sodium citrate and $AgNO_3$ were purchased from Tianjin Guangfu Technology development Co., Ltd.

The fabrication of the ZnOs: firstly, $C_4H_6O_4Zn{\bullet}2H_2O$ (2.5 mM) and sodium citrate (2.5 mM) were dissolved into 40 mL deionized water under stirring until a clear aqueous solution was obtained. Secondly, 4 mL of NaOH with concentration of 1.0 M, 1.5 M and 4.0 M were added separately into the prepared aqueous solution with rigorous stirring to obtain white colloidal solutions. Then, the mixtures were transferred into separated Teflon liner stainless-steel autoclaves (70 mL) and heated at 120 °C for 8 h. After cooling to room temperature, the precipitates were washed repeatedly with deionized water and ethanol before drying at 60 °C for 2 h. The obtained samples using different concentrations of NaOH (1.0 M, 1.5 M and 4.0 M) were labelled as ZnOb, ZnOf and ZnOs, respectively.

The fabrication of the Ag-NPs/ZnOs composite: firstly, to obtain the activated ZnOs, 30 mg ZnOs was placed in 10 mL 0.03 mM $SnCl_2$ ethanol solution with vigorously stirred for about 30 min followed by centrifugation. Secondly, to obtain the ZnOs decorated with Ag seeds, the activated ZnOs were dispersed in 10 mL ethanol containing 10 mg of $AgNO_3$ with continuous stirring for 15 min followed by centrifugation. Thirdly, to assemble Ag-NPs onto the ZnOs surface, the above obtained products was dispersed in a 0.01 M $Ag(NH_3)_2^+$ solution, while in another flask, 0.4 mL of formaldehyde solution, 0.4 mL of deionized water and 9.2 mL of ethanol were mixed. Finally, 0.5 mL of the mixture solution was added into the $Ag(NH_3)_2^+$ solution with ZnOs decorated with Ag seeds drop by drop with stir for 15 min, and the precipitate was collected by centrifugation and washed with deionized water and ethanol. After drying in vacuum at 50 °C for 12 h, the Ag-NPs/ZnOs product was finally obtained.

2.2. Characterization

Field emission scanning electron microscope (FESEM, Sirion 200 FEG) and transmission electron microscopy (TEM, JEOL-2010) with an energy dispersive X-ray spectrometer (EDX) were used to characterize the structural morphology and the elements distribution. The crystalline phases were identified by X-ray diffractometry (XRD, Philips Xpert PRO) using the Ni-filtered monochromatic Cu Kα radiation at 40 keV and 40 mA. X-Ray photoelectron spectroscopy (XPS) was performed by a Thermo ESCALAB 250 photoelectron spectrometer with Al Kα X-rays as the excitation source. Ag content in the composite structure was determined by the inductively coupled plasma spectroscopy (ICP6300, Thermo Fisher Scientific). Nitrogen adsorption at 77 K (Micrometrics ASAP 2020M) was used to measure surface area of the products. The UV-Vis absorption spectra of the samples were characterized by spectrophotometer (CARY-5E). Room-temperature fluorescent was measured by a confocal microprobe Raman system (LABRAM-HR, France) using 325 nm laser.

2.3. Photocatalytic activity measurement

To evaluate the photocatalytic activity of the samples, photodegradation of organic dyes, methylene blue (MB) and methyl orange (MO), were investigated. A 300 W UV lamp with maximum emission at 365 nm was used as the UV resource. In a typical test, 20 mg of the as-prepared photocatalyst powders (i.e. ZnOb, ZnOf, ZnOs or Ag-NPs/ZnOs) was suspended in the organic dye (1.25×10^{-5} M, 80 mL) aqueous solution. After the stir for 30 min in dark to reach an adsorption–desorption equilibrium between the photocatalyst and organic dye, the solution was irradiated in a photochemical reaction chamber with continuous stirring. At a certain time interval, 3 mL treated solution was taken out and centrifuged at 7000 rpm for 2 min. The relative concentration of organic dye in the treated solution was evaluated by the intensity of the UV–Vis absorption peaks.

2.4. Electrochemical measurement

A three-electrode electrochemical cell was employed to construct cyclic voltammetry curves and for electrochemical impedance spectra (EIS) measurements in which a platinum filament served as counter electrode and a saturated Ag/AgCl served as reference electrode. The current versus voltage (C–V) curves of the as-prepared bare ZnOs and Ag-NPs/ZnOs composite electrode were measured between the −1.2 V and 0.5 V at a scan rate of 20 mV/S. The EIS spectra were obtained by applying an open-circuit voltage in the frequency range of 100 KHz to 0.1 Hz with oscillation amplitude of 50 mV. Before performing the EIS test, the test cell was discharged to a designated potential, and was kept at open-circuit condition for 1 h to ensure that the cell was in equilibrium. All the electrochemical measurements were done using a Zahner IM6e Electrochemical Workstation in the 0.1 M Na_2SO_4 solution.

3. Results and discussion

3.1. Structure and morphology

As shown in Fig. 1a, the as-prepared ZnOs are uniform-distributed flower-like microspheres with diameter ranging from 2 to 3 μm. And, these ZnO microspheres are assembled with ZnO nanosheets with 25 nm in thickness and 1 μm in width, as shown in

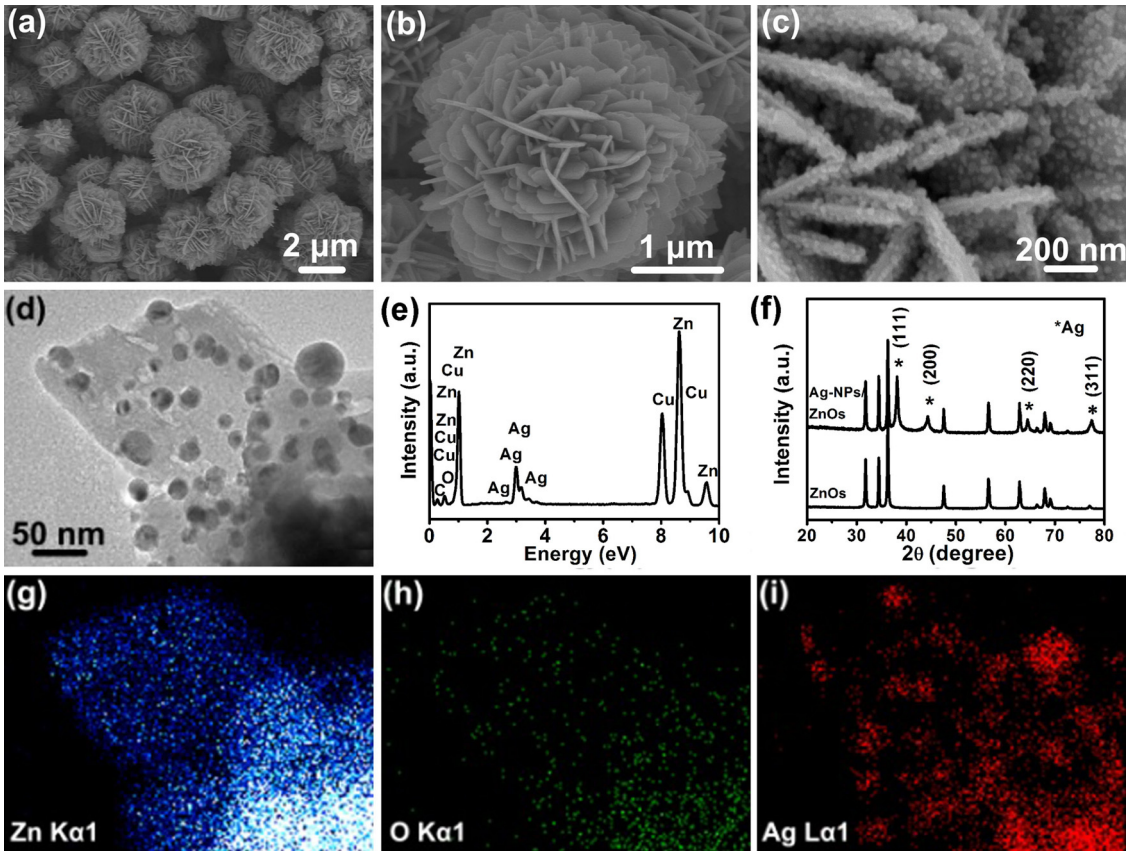

Fig. 1. (a) SEM image and (b) enlarged view of the as-prepared ZnOs. (c) high magnified SEM image and (d) HRTEM image of the as-prepared Ag-NPs/ZnOs. (e) the EDX spectrum of the sheet shown in 1(d). (f) XRD patterns of the as-prepared bare ZnOs and the Ag-NPs decorated ZnOs. The elemental mapping images of elemental (g) Zn, (h) O and (i)Ag.

Fig. 1b for the enlarged view of the ZnOs. The micro/nanostructure character of the ZnOs ensures the high structural stability and high activity of nano-size ZnO nanosheets. The high magnification SEM image (Fig. 1c) and TEM image (Fig. 1d) of Ag-NPs/ZnOs reveal that the Ag-NPs with a diameter of 15–50 nm have been dispersed uniformly onto the whole surface of each ZnO nanosheets with high density. The EDX of the composite sheet shown in Fig. 1d confirms that the Zn, Ag, O, C and Cu elements co-existed (shown in Fig. 1e), where the Ag, Zn and O signals are originated from the Ag-NPs/ZnOs composite structure while the C and Cu signal is from the carbon film and copper grid, respectively. The spatial distribution of different compositional elements was clarified by elemental mappings (Fig. 1e–g) using Zn Kα1 edge (8631 eV), O Kα1 edge (525 eV) and Ag Lα1 edge (2984 eV), respectively. The spatial distribution of Ag is similar with that of Zn and O, which further demonstrate that high density of Ag-NPs have been uniformly decorated onto the surface of the flower-like ZnOs.

The phase characters of the as-prepared bare ZnOs and Ag-NPs/ZnOs are revealed in Fig. 1f. The peaks of typical hexagonal wurtzite structure of ZnO (JCPDS Card no. 36-1451) are observed in the patterns of the two samples. For the Ag-NPs/ZnOs, the four additional peaks, (1 1 1), (2 0 0), (2 2 0) and (3 1 1) peaks labelled with * in Fig. 1f, can be assigned to the fcc Ag in the sample (JCPDS Card no. 04-0783). In order to quantify the content of Ag in the sample, the Ag-NPs/ZnOs is dispersed in 5 mL of distilled water and dissolved by addition of nitric acid, and the Ag content in the solution is determined by the inductively coupled plasma spectroscopy (ICP). As shown in Table S1 of supporting information, the content of the Ag reaches to 25.7 wt%, revealing the large amount of Ag-NPs on the surface of the ZnOs.

The specific surface area and pore size distribution of the ZnOs and Ag-NPs/ZnOs samples is presented in Table S2 and Fig. S1. via nitrogen adsorption/desorption measurements. The calculated specific surface area (SBET) is 10.23 m^2/g for ZnOs, much larger than that for ZnOb (4.81 m^2/g) and ZnOf (5.37 m^2/g). After the decoration of the Ag-NPs, the SBET is increased to 14.02 m^2/g. However, the pore size distribution of Ag-NPs/ZnOs has no obvious changes compared with the bare ZnOs, as shown in Fig.S1. The reason can be found that the Ag-NPs are localized at the ZnO nanosheets and thus the new pore structures are formed between the Ag-NPs. It is known that large specific surface area is more favourable to absorb targeted molecules. Thus, the enhanced SBET of the flower-like ZnOs and the Ag-NPs/ZnOs will be helpful to improve the photocatalytic activity of the Ag-NPs/ZnOs.

3.2. Growth mechanism of ZnOs

The presence of citrate ions and the concentration of sodium hydroxide play key roles in the formation of ZnOs, which are revealed via two groups controlled trials. In the controlled experiments without sodium citrate, thick ZnO rods, ZnO clusters, and ZnO hexagonal rods are obtained with 1.0 M, 1.5 M and 4.0 M NaOH, respectively, as shown in Fig. S2. From the previous literature, the quantity of $Zn(OH)_2$ and the growth unit $[Zn(OH)_4]^{2-}$, which contribute respectively to nuclei and growth of ZnO, would be affected by the amount of NaOH [22]. The related reaction equations are listed below [23]:

$$Zn^{2+} + 2OH^- \rightarrow Zn(OH)_2\downarrow \quad (1)$$

$$Zn(OH)_2 + 2OH^- \rightarrow Zn(OH)_4{}^{2-} \quad (2)$$

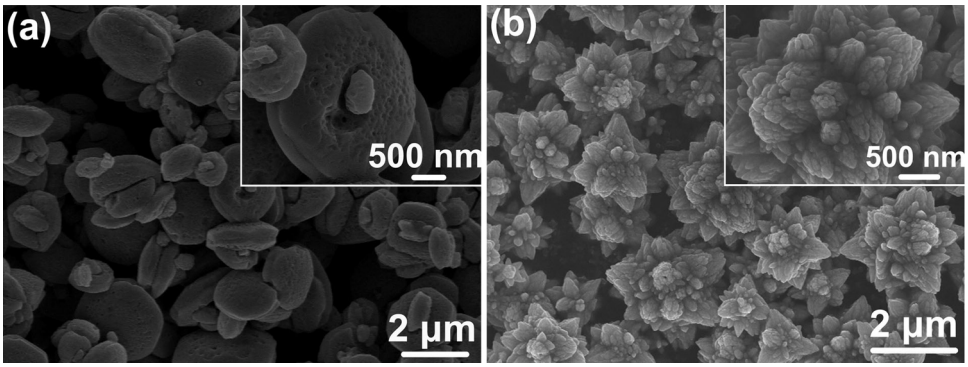

Fig. 2. SEM images of the as-prepared ZnO samples with different concentrations of NaOH: (a) 1.0 M, (b) 1.5 M (the inset shows the enlarged image).

$$Zn(OH)_4^{2-} \leftrightarrow ZnO + 2H_2O + 2OH^- \quad (3)$$

While adding NaOH into the Zn^{2+} solution, if the amount of NaOH is less than Zn^{2+}, Eq. (1) will be occurred. As more NaOH is added, when the amount of NaOH is two times more and four times less than the amount of Zn^{2+} (i.e. $2n(Zn^{2+}) < n(NaOH) < 4n(Zn^{2+})$), $Zn(OH)_2$ starts to dissolve and form the $[Zn(OH)_4]^{2--}$ according to Eqs. (1) and (2). When adding 1.5 M of NaOH (i.e. n(NaOH) = 6 mmol), a larger quantity of $Zn(OH)_2$ and a smaller quantity of $[Zn(OH)_4]^{2--}$ will be obtained. This implies that the quantity of the corresponding ZnO nuclei is larger, while there is not enough $[Zn(OH)_4]^{2-}$ to seed the ZnO nuclei [22]. As a result of the anisotropic growth of ZnO, tip-like ZnO particles are obtained (shown in Fig. S2b). However, when the concentration of NaOH is reduced to 1.0 M, i.e. n(NaOH) = 4 mmol and $n(NaOH) < 2n(Zn^{2+})$, majority of $Zn(OH)_2$ precipitates will not be dissolved and consequently hexagonal ZnO nuclei with a side length of 1~2 μm are produced (shown in Fig. S2a). The thick ZnO rods are obtained during the hydrothermal process because of the inadequate OH^-. As the concentration of NaOH increases to 4 M, i.e. n(NaOH) = 16 mmol and $n(NaOH) > 4n(Zn^{2+})$, a smaller quantity of $Zn(OH)_2$ and a larger quantity of $[Zn(OH)_4]^{2-}$ are produced. Therefore, the amount of ZnO nuclei will be less. In such a case, there is enough growing unit of $[Zn(OH)_4]^{2-}$ to facilitate ZnO nanorods being grown from the circumference of the ZnO nuclei. Thus the flower-like ZnO bundles consisting of ZnO hexagonal rods are obtained (shown in Fig. S2c) [22].

However, once the sodium citrate is added in the synthesis solution, the results are quite different. The morphologies of the obtained ZnO products synthesized with 2.5 mM sodium citrate and 1.0 M, 1.5 M and 4.0 M NaOH are shown in Fig. 2a,b and Fig. 1b, respectively. As shown in Fig. 2a, double-layer bread-like ZnO structures (ZnOb) with rough surface (as shown in the inset) have been achieved with low concentration NaOH. The average diameter is about 500 nm–2000 nm. As shown in Fig. 2b, flower-like cluster ZnO structures with 1000 nm–3000 nm in diameter which are composed of irregular particles (as shown in the inset) have been achieved with moderate concentration NaOH. As shown in Fig. 1b, the ZnO nanosheets assembled ZnOs have been achieved with high concentration NaOH. Fig. S3 shows the XRD patterns of the as-prepared ZnO with different morphologies, and the peaks are of typical hexagonal wurtzite structure of ZnO (JCPDS Card no. 36-1451). It can be seen that the sodium citrate is vital in the formation of ZnOs, besides the high concentration of NaOH. In the synthesis, the citrate ions serve as surface modifier, bonding to the Zn^{2+} (0 0 0 1) surfaces via the —COO— and —OH functions [24], and such surface interaction can inhibit the growth of ZnO crystals being perpendicular to the planes [25,26]. On the other hand, the complexation effect of citrate ions with Zn^{2+} postpones the combination of Zn^{2+} with hydroxide ions and controls the precipitation process [26,27].

3.3. Chemical compositions of the ZnO structures and Ag-NPs/ZnOs samples

The surface chemical compositions of the three bare ZnO structures with different morphology and the as-prepared Ag-NPs/ZnOs composite structures are investigated via XPS analysis. The binding energies in the XPS spectra are calibrated by using that of C 1s (284.8 eV). The XPS spectra of O 1s and Zn 2p for ZnOb, ZnOf, and ZnOs structures are shown in Fig. S4. For the spectrum of ZnOs, the O 1s can be fitted to two symmetrical peaks (α and β), indicating two different O species in the ZnOs. The peaks of α and β are related to the lattice oxygen (Ol) [28,29], and the chemi-sorbed oxygen (Oa) of ZnO as a result of surface hydroxyl [30]. The symmetric peak centered at 1021.4 eV in Fig. S4f is attributed to Zn $2p_{3/2}$ [17]. The same results are observed for the other two ZnO structures samples, suggesting that the three ZnO structures have the same chemical compositions. The surface atomic ratio between Ol and Zn (Ol/Zn) is calculated from the results of the XPS spectra and the peak area ratio of α/β. The related results are shown in Table S3. The calculated Ol/Zn ratios are found to be 0.70, 0.58 and 0.73 for ZnOb, ZnOf and ZnOs, respectively, which reveals that these samples are oxygen deficient [17].

The XPS spectra of the as-prepared Ag-NPs/ZnOs composite photocatalyst are shown in Fig. 3. There are no peaks related to other elements excepted for Zn, O, Ag and C. These elements are observed in the XPS spectra in Fig. 3a, which further confirms that the pure Ag-NPs have been deposited successfully onto the surface of the as-prepared ZnOs. The C element mainly comes from the carbon oxide in air adsorbed on the surface of the ZnOs samples. The high-resolution spectrum of Ag in the Ag-NPs/ZnOs sample is shown in Fig. 3b. The Ag $3d_{5/2}$ peak appears at the binding energy of 367.5 eV and the splitting of the 3d doublet is 6.0 eV, indicating the presence of metallic silver [28]. The Ag $3d_{5/2}$ and Ag $3d_{3/2}$ peaks are shifted to the lower binding energy differing from the standard values (about 368.2 and 374.2 eV for bulk Ag), which is owing to the transfer of electrons from Ag-NPs to the ZnO nanosheets at the interfaces of the heterostructures [8,9,17,19]. The peak in Fig. 3c is assigned to Zn $2p_{3/2}$. The O 1s for Ag-NPs/ZnOs are also fitted to the α and β peaks (corresponding to the Ol and Oa), and the detailed XPS analysis results are calculated and listed in Table S3. It should be mentioned that the Ol/Zn ratio is improved to be 0.93 after modification with Ag-NPs compared with 0.73 for the bare ZnOs, indicating the reduction of the oxygen defect density for the surface decoration of Ag-NPs.

Fig. 4 shows the room-temperature PL spectra of the as-prepared bare ZnOs and Ag-NPs/ZnOs composite photocatalyst. A

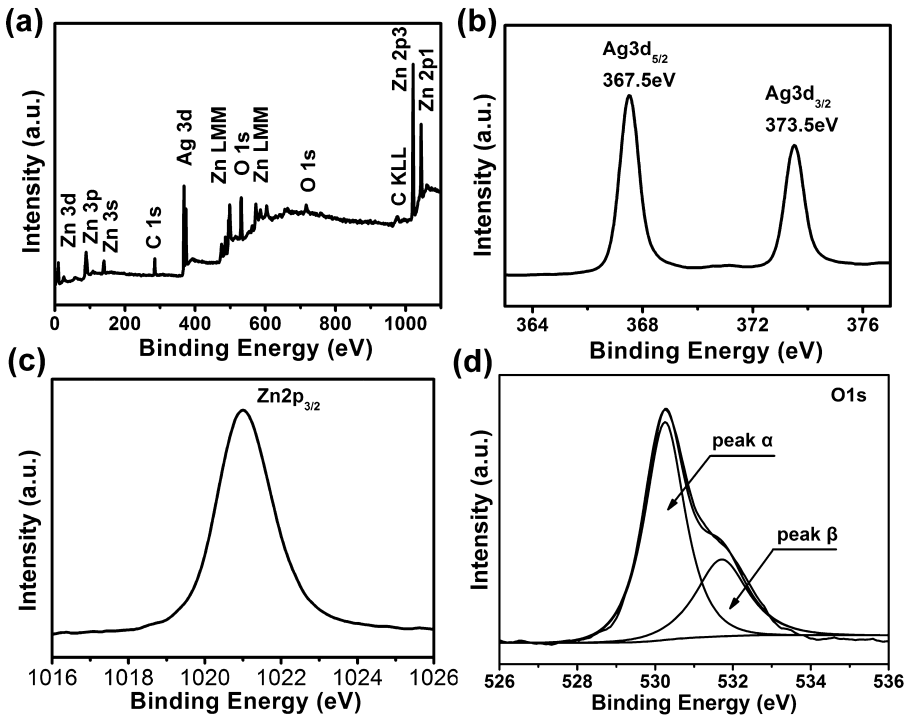

Fig. 3. (a) Full XPS spectra, (b) Ag 3d spectra, (c) Zn $2p_{3/2}$ spectra and (d) O 1s spectra of the as-prepared Ag-NPs/ZnOs composite photopcatalyst.

strong UV emission peak at ~385 nm and a negligible green band are observed in the PL spectrum of Ag-NPs/ZnOs, while there is strong UV emission peak and a strong green band (500–700 nm) in the spectrum of the bare ZnOs. The UV emission can be assigned to the near-band-edge emission of the band gap of ZnO, while the green emission is a common defect emission in the nanostructured ZnO, attributed to the defect state located at the surface of nanostructured ZnO [31], i.e. the singly ionized oxygen vacancy in ZnO [32], oxygen vacancies, and the zinc interstitials [33]. Therefore, the weakening of the green emission in the PL spectrum of the Ag-NPs/ZnOs compared with the bare ZnOs implies the modification of Ag-NPs reduces the optical effects, especially the surface oxygen defects [34], which is in agreement with the results obtained by the XPS analysis. The photo-corrosion (one of the main factor to decrease the photocatalytic activity) mainly occurred at the surface defect sites of ZnO [35,36], thus the reduction of the amount of surface defects in the Ag-NPs/ZnOs composite photocatalyst can be feasible to effectively inhibit the photo-corrosion. Additionally, the diffuse-reflectance UV–vis spectra of the as-prepared bare ZnOs and Ag-NPs/ZnOs hybrid photocatalyst are shown in Fig. S5 in Supporting Information. The absorption edge located around 389 nm is assigned to the absorption of ZnO semiconductor, while the absorption band located at around 448 nm is attributed to the characteristic absorption of surface plasmon resulting from the metallic Ag-NPs in the Ag-NPs/ZnOs heterostructure.[37,38]

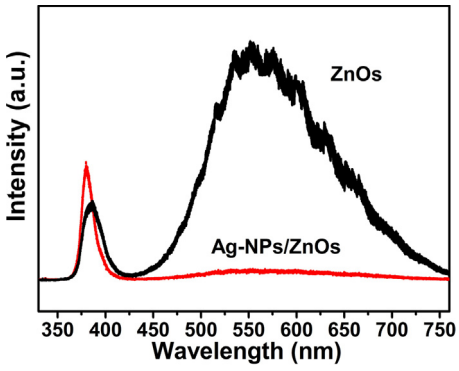

Fig. 4. PL spectra of the as-prepared bare ZnOs and the Ag-NPs/ZnOs composites.

3.4. Photocatalytic performances of the samples

The photocatalytic performances in the UV region are demonstrated via degradation of MB and MO, the two typical organic pollutants commonly generated by the textile industry. The degradation rates of MB and MO under UV irradiation using the as-prepared three bare ZnO photocatalysts with different morphologies (ZnOb, ZnOf and ZnOs) are shown in Fig. 5a–c, respectively. The controlled experiments without photocatalysts are also presented in the same figure, showing the self-degradation effect of the organic pollutants under UV irradiation (less than 13% and 8% for MB and MO, respectively). In the figures, C is the concentration of organic pollutants remaining in the solution after irradiation duration of t, and C_0 is the initial concentration at $t = 0$. It is obviously observed that the degradation rate of both MB and MO molecules by using ZnOs is higher than the ZnOb and ZnOf in the given time. The photocatalytic degradation kinetic reaction could be interpreted by the pseudo-first-order kinetics [1,9], $\ln(C_0/C) = kt$, where k is a pseudo-first-rate kinetic constant and t is irradiation time. The values of the squares of linear correlation coefficients (R^2) are larger than 0.97 (see in Table 1), thus the photodegradation of MB and MO can follow a pseudo-first-order reaction; and the slope of the linear curve should be the rate constant k. The variation of $\ln(C_0/C)$ as a function of irradiation time are shown in Fig. 5b and d. The calculated k value for the as-prepared ZnOb, ZnOf and ZnOs are listed in Table 1. It should be mentioned that the k value of the ZnOs in degrading MB is 9.31 times and 4.43 times larger than that of the ZnOb and ZnOf, respectively; while in degrading MO, is 10.05 and 5.59 times larger, respectively. The enhancement photocatalytic activity of the ZnOs compared with the ZnOb and ZnOf can be attributed to the larger specific surface area of the ZnOs

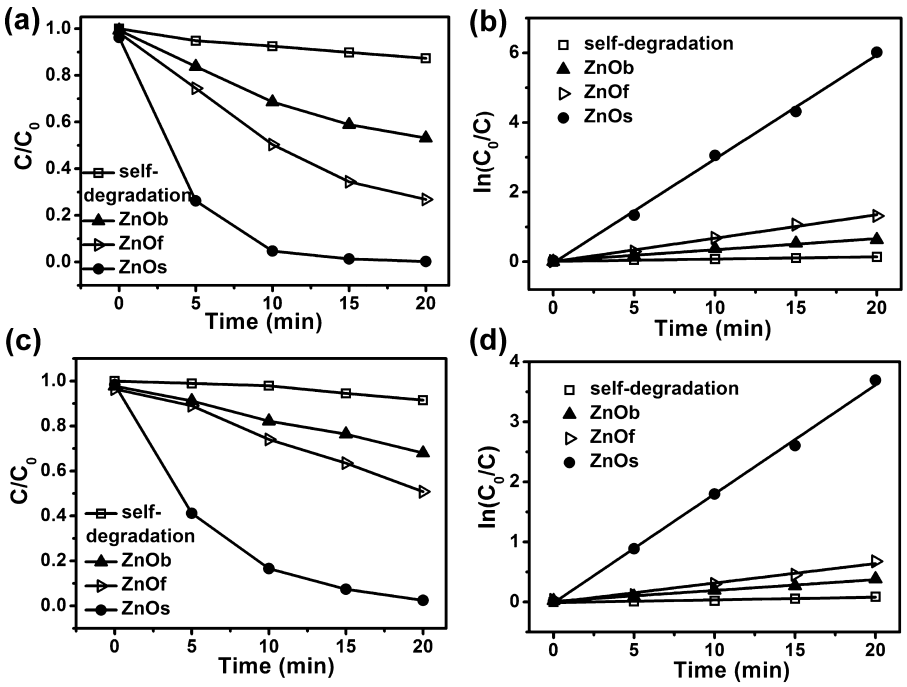

Fig. 5. The photocatalytic performances of the different bare ZnO structures samples for degradation of MB (a, b) and MO (c, d) under UV irradiation (the uppermost curves show the self-degradation of the dyes without photocatalyst as control group).

(shown in Table S2) induced by morphology difference shown in Fig.1b and Fig. 2.

The photocatalytic activity and kinetics of the as-prepared bare ZnOs and the Ag-NPs/ZnOs composite structures for degradation of MB and MO are presented in Fig. 6. As shown in Fig. 6a, MB can be almost degraded in 15 min by bare ZnOs; but only in 7 min by Ag-NPs/ZnOs composite photocatalyst. Also, nearly 20 min is needed for bare ZnOs to completely degrade the MO, but only about 9 min for the Ag-NPs/ZnOs composite photocatalyst. The calculated k values for the degradation of MB and MO using the as-prepared bare ZnOs and the Ag-NPs/ZnOs are listed in Table 2. The k value of the Ag-NPs/ZnOs is 1.57 times and 2.01 times larger than that of the bare ZnOs and in degrading MB and MO, respectively. Consequently, after the surface decoration of the Ag-NPs, the Ag-NPs/ZnOs composite structures show higher photocatalytic activity than the bare ZnOs.

To investigate the stability of photocatalytic performance of the as-prepared Ag-NPs/ZnOs, i.e. the reusability, photocatalytic

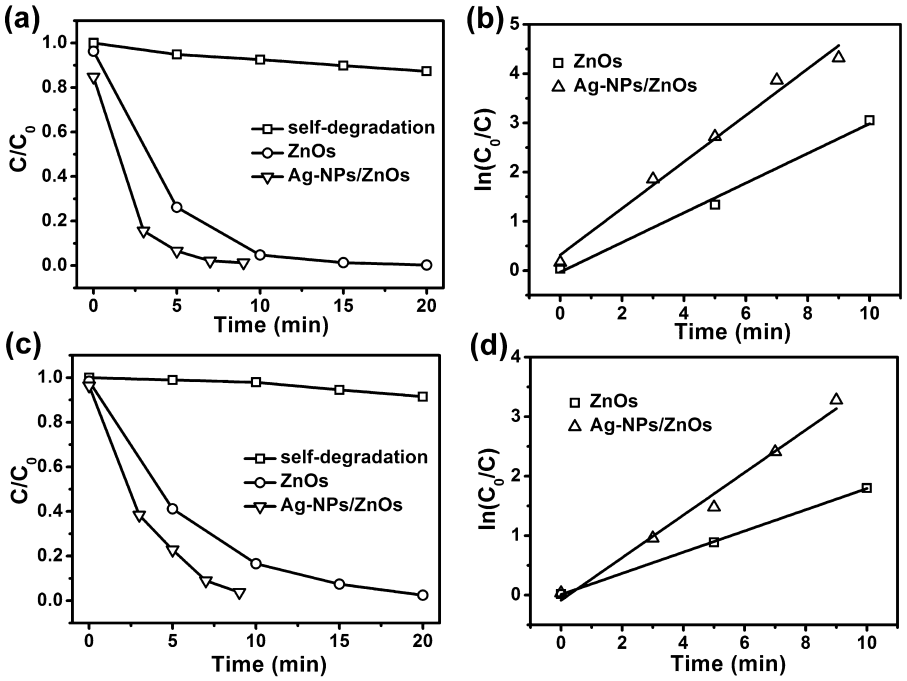

Fig. 6. The photocatalytic activity and kinetics of the as-prepared bare ZnOs and the Ag-NPs/ZnOs for degradation of (a, b) MB and (c, d) MO under UV irradiation (the uppermost curves show the self-degradation of the dyes without photocatalyst as control group).

Table 1
Reaction rate constants (k) for photocatalytic degradation of MB and MO over different ZnO photocatalysts under UV irradiation. (R^2 represents the square of correlation coefficient of kinetics linear fitting).

	UV	ZnOb	ZnOf	ZnOs
MB	k/min^{-1}	0.03209	0.06737	0.29874
	R^2	0.98427	0.99245	0.99685
MO	k/min^{-1}	0.01806	0.03244	0.18145
	R^2	0.99078	0.97227	0.99718

Table 2
Reaction rate constants (k) for photocatalytic degradation of MB and MO using the bare ZnOs and the Ag-NPs/ZnOs under UV irradiation.

	UV	ZnOs	Ag-NPs/ZnOs
MB	k/min^{-1}	0.30148	0.47262
	R^2	0.98759	0.98058
MO	k/min^{-1}	0.17825	0.35782
	R^2	0.99967	0.9816

degradation cycles of MB is measured and shown in Fig. 7. The photocatalytic efficiency hardly reduced (less than 2.5%) after four cycles, demonstrating high photostability potentials. The structural stability as a result of the micro/nanostructure character of the as-prepared Ag-NPs/ZnOs photocatalysts is mainly responsible for the favourable photostability.

3.5. Electrochemical responses in C–V and EIS measurements

As the photocatalytic activity of the semiconductor mainly depends on the direct electron transfer rate and the interface charge separation efficiency of photogenerated electrons and holes. Then, the two characters of the as-prepared Ag-NPs/ZnOs composite photocatalyst are investigated with electrochemical methods. Fig. 8a shows the C–V curves of electrodes fabricated with the bare ZnOs and the Ag-NPs/ZnOs composite photocatalyst powders in 0.1 M Na_2SO_4 solution. With scan range from −1.2 V to 0.5 V, the bare ZnOs electrode displays hardly any reaction, as revealed by the solid line in Fig. 8a. In contrary, the Ag-NPs/ZnOs electrode presents a much more obvious current response. Fig. 8b shows the EIS Nyquist plots of electrode in a defined electrolyte of 0.1 M Na_2SO_4. The radius of the arc on the EIS spectra reveal the interface layer resistance occurring at the surface of electrode, and smaller arc radius implies higher efficiency of charge transfer [39]. It is observed that the arc radius of the Ag-NPs/ZnOs (inset of Fig. 8b) is much smaller than that of ZnOs, which indicates more rapid charge transfer in the Ag-NPs/ZnOs composite photocatalyst. These results demonstrate that the introduction of Ag-NPs to ZnOs has dramatically enhanced the transportation rate of surface electrons through an interfacial

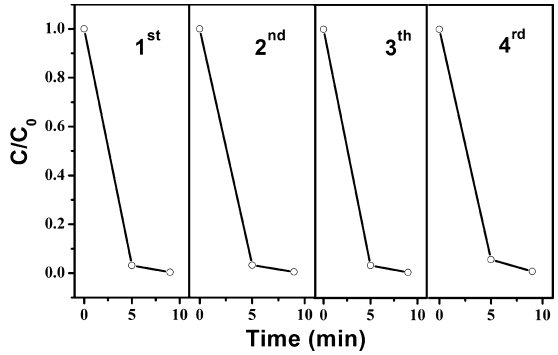

Fig. 7. Four photocatalytic degradation cycles of MB using the as-prepared Ag-NPs/ZnOs photocatalysts.

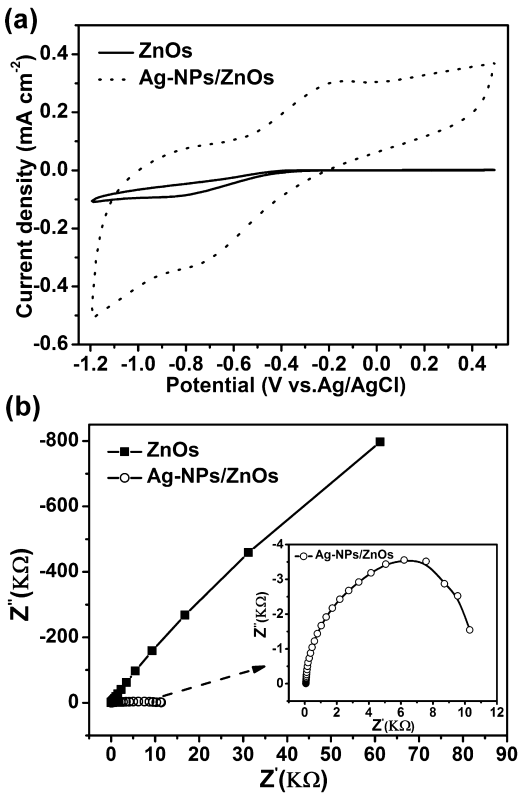

Fig. 8. (a) C–V curves of the as-prepared ZnOs and Ag-NPs/ZnOs electrode in 0.1 M Na_2SO_4 solution. (b) EIS measured with the ZnOs and the Ag-NPs/ZnOs electrode in 0.1 M Na_2SO_4 solution (the inset shows the high-magnification view of EIS measured with the Ag-NPs/ZnOs electrode).

interaction between ZnO nanosheets on the ZnOs and the Ag-NPs. This further improves the surface activities for photocatalysis.

3.6. Mechanism of enhanced catalytic activity of the composite Ag-NPs/ZnOs

The catalytic process by activation of UV irradiation or the external potential bias is illustrated in Scheme 1. The enhanced photocatalytic performance in UV region is attributed to the formation of the Schottky barriers at metal–semiconductor interface between the Ag-NPs and the nanosheets of the ZnOs, which improve the segregation of charges and prevent the charge recombination [19,40–43]. The Ag-NPs/ZnOs photocatalysis under UV irradiation include multiple steps, e.g. the formation of the Schottky barriers at metal-semiconductor interaction; excitation of ZnOs by UV light; generation of electron-hole pairs; generation of reactive oxidative species (ROSs) and mineralization of the organic compounds by ROSs [10,44]. In this study, the interfacial interactions

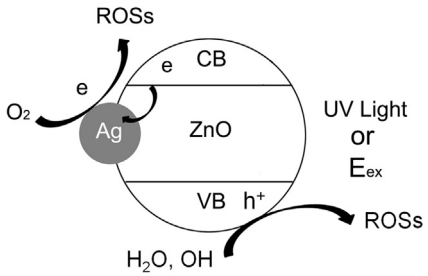

Scheme 1. The schematic diagram to illustrate the degradation process of MB or MO pollutants by using the Ag-NPs/ZnOs under UV irradiation.

between ZnOs and highly dispersed Ag-NPs could dramatically enhance the separation and transfer efficiency of photogenerated e–h pairs as demonstrated in the C–V and EIS measurements.

4. Conclusions

A new micro/nanostructure photocatalyst with enhanced photocatalytic performances have been fabricated via decorating highly dispersed Ag-NPs onto the surface of the flower-like ZnO nanosheets assembled microspheres. The as-prepared Ag-NPs/ZnOs have shown enhanced photocatalytic activity in MB and MO degradation under UV irradiation. The enhanced photocatalytic activity could be attributed to the enhanced transportation rate of surface electrons and separation efficient of the electron–hole pairs induced by the decorated Ag-NPs, which are demonstrated by electrochemical characterizations (C–V and EIS spectra).

Acknowledgement

This work was supported by the Natural Science Foundation of China (Grant No. 51072199).

Appendix A. Supplementary data

Supplementary data associated with this article can be found, in the online version, at http://dx.doi.org/10.1016/j.apsusc.2014.12.202.

References

[1] M.J. Height, S.E. Pratsinis, O. Mekasuwandumrong, P. Praserthdam, Ag-ZnO catalysts for UV-photodegradation of methylene blue, Appl. Catal. B: Environ. 63 (2006) 305–312.
[2] R.B. Jiang, B.X. Li, C.H. Fang, J.F. Wang, Metal/semiconductor hybrid nanostructures for plasmon-enhanced applications, Adv. Mater. 26 (2014) 5274–5309.
[3] M. Pudukudy, Z. Yaakob, Simple chemical synthesis of novel ZnO nanostructures: Role of counter ions, Solid State Sci. 30 (2014) 78–88.
[4] M. Pudukudy, Z. Yaakob, Hydrothermal synthesis of mesostructured ZnO micropyramids with enhanced photocatalytic performance, Superlattice Microst. 63 (2013) 47–57.
[5] M. Pudukudy, Z. Yaakob, Facile solid state synthesis of ZnO hexagonal nanogranules with excellent photocatalytic activity, Appl. Surf. Sci. 292 (2014) 520–530.
[6] M. Pudukudy, A. Hetieqa, Z. Yaakob, Synthesis, characterization and photocatalytic activity of annealing dependent quasi spherical and capsule like ZnO nanostructures, Appl. Surf. Sci. 319 (2014) 221–229.
[7] M. Pudukudy, Z. Yaakob, R. Rajendran, T. Kandaramath, Photodegradation of methylene blue over novel 3D ZnO microflowers with hexagonal pyramid-like petals, React. Kinet. Mech. Catal. 112 (2014) 527–542.
[8] D.D. Lin, H. Wu, R. Zhang, W. Pan, Enhanced photocatalysis of electrospun Ag-ZnO heterostructured nanofibers, Chem. Mater. 21 (2009) 3479–3484.
[9] Y.L. Lai, M. Meng, Y.F. Yu, One-step synthesis, characterizations and mechanistic study of nanosheets-constructed fluffy ZnO and Ag/ZnO spheres used for Rhodamine B photodegradation, Appl. Catal. B: Environ. 100 (2010) 491–501.
[10] W.W. Lu, S.Y. Gao, J.J. Wang, One-pot synthesis of Ag/ZnO self-assembled 3D hollow microspheres with enhanced photocatalytic performance, J. Phys. Chem. C 112 (2008) 16792–16800.
[11] W.B. Li, F.X. Hua, J.G. Yue, J.W. Li, Ag@AgCl plasmon-induced sensitized ZnO particle for high-efficiency photocatalytic property under visible light, Appl. Surf. Sci. 285 (2013) 490–497.
[12] B. Divband, M. Khatamian, G.R.K. Eslamian, M. Darbandi, Synthesis of Ag/ZnO nanostructures by different methods and investigation of their photocatalytic efficiency for 4-nitrophenol degradation, Appl. Surf. Sci. 284 (2013) 80–86.
[13] F. Lu, W.P. Cai, Y.G. Zhang, ZnO hierarchical micro/nanoarchitectures: Solvothermal synthesis and structurally enhanced photocatalytic performance, Adv. Funct. Mater. 18 (2008) 1047–1056.
[14] X.Z. Li, F.B. Li, Study of Au/Au^{3+}-TiO_2 photocatalysts toward visible photooxidation for water and wastewater treatment, Environ. Sci. Technol. 35 (2001) 2381–2387.
[15] A.L. Linsebigler, G.Q. Lu, J.T. Yates, Photocatalysis on TiO_2 surfaces - principles, mechanisms, and selected results, Chem. Rev. 95 (1995) 735–758.
[16] H. Tada, K. Teranishi, Y. Inubushi, S. Ito, Ag nanocluster loading effect an TiO_2 photocatalytic reduction of bis(2-dipyridyl)disulfide to 2-mercaptopyridine by H_2O, Langmuir 16 (2000) 3304–3309.
[17] Y.H. Zheng, L.R. Zheng, Y.Y. Zhan, X.Y. Lin, Q. Zheng, K.M. Wei, Ag/ZnO heterostructure nanocrystals: synthesis, characterization, and photocatalysis, Inorg. Chem. 46 (2007) 6980–6986.
[18] J. Mu, Y.Y. Zhang, One-pot synthesis, photoluminescence, and photocatalysis of Ag/ZnO composites, J. Colloid. Interf. Sci. 309 (2007) 478–484.
[19] J. Rodriguez-Fernandez, A.M. Funston, J. Perez-Juste, R.A. Alvarez-Puebla, L.M. Liz-Marzan, P. Mulvaney, The effect of surface roughness on the plasmonic response of individual sub-micron gold spheres, Phys. Chem. Chem. Phys. 11 (2009) 5909–5914.
[20] Q. Deng, X.W. Duan, D.H.L. Ng, H.B. Tang, Y. Yang, M.G. Kong, Z.K. Wu, W.P. Cai, G.Z. Wang, Ag nanoparticle decorated nanoporous ZnO microrods and their enhanced photocatalytic activities, ACS Appl. Mater. Inter. 4 (2012) 6030–6037.
[21] Y.H. Zheng, C.Q. Chen, Y.Y. Zhan, X.Y. Lin, Q. Zheng, K.M. Wei, J.F. Zhu, Photocatalytic activity of Ag/ZnO heterostructure nanocatalyst: Correlation between structure and property, J. Phys. Chem. C 112 (2008) 10773–10777.
[22] H. Zhang, D. Yang, X.Y. Ma, Y.J. Ji, J. Xu, D.L. Que, Synthesis of flower-like ZnO nanostructures by an organic-free hydrothermal process, Nanotechnology 15 (2004) 622–626.
[23] J.R. Huang, Y.J. Wu, C.P. Gu, M.H. Zhai, K. Yu, M. Yang, J.H. Liu, Large-scale synthesis of flowerlike ZnO nanostructure by a simple chemical solution route and its gas-sensing property, Sensor. Actuat. B: Chem. 146 (2010) 206–212.
[24] Z.R.R. Tian, J.A. Voigt, J. Liu, B. Mckenzie, M.J. Mcdermott, Biommetic arrays of oriented helical ZnO nanorods and columns, J. Am. Chem. Soc. 124 (2002) 12954–12955.
[25] W.J. Li, E.W. Shi, W.Z. Zhong, Z.W. Yin, Growth mechanism and growth habit of oxide crystals, J. Cryst. Growth 203 (1999) 186–196.
[26] J.B. Liang, J.W. Liu, Q. Xie, S. Bai, W.C. Yu, Y.T. Qian, Hydrothermal growth and optical properties of doughnut-shaped ZnO microparticles, J. Phys. Chem. B 109 (2005) 9463–9467.
[27] X.G. Peng, Mechanisms for the shape-control and shape-evolution of colloidal semiconductor nanocrystals, Adv. Mater. 15 (2003) 459–463.
[28] J.F. Moudler, W.F. Stickle, P.E. Sobol, K.D. Bomben, Handbook of X-ray Photoelectron Spectroscopy, Physical Electronics Division, Perkin-Elmer: Eden Prairie, 1992.
[29] W.Q. Peng, S.C. Qu, G.W. Cong, Z.G. Wang, Synthesis and structures of morphology-controlled ZnO nano- and microcrystals, Cryst. Growth Des. 6 (2006) 1518–1522.
[30] L.Q. Jing, Z.L. Xu, J. Shang, X.J. Sun, W.M. Cai, H.C. Guo, The preparation and characterization of ZnO ultrafine particles, Mat. Sci. Eng. A-Struct. 332 (2002) 356–361.
[31] A.B. Djurisic, Y.H. Leung, Optical properties of ZnO nanostructures, Small 2 (2006) 944–961.
[32] K. Vanheusden, W.L. Warren, C.H. Seager, D.R. Tallant, J.A. Voigt, B.E. Gnade, Mechanisms behind green photoluminescence in ZnO phosphor powders, J. Appl. Phys. 79 (1996) 7983–7990.
[33] X. Liu, X.H. Wu, H. Cao, R.P.H. Chang, Growth mechanism and properties of ZnO nanorods synthesized by plasma-enhanced chemical vapor deposition, J. Appl. Phys. 95 (2004) 3141–3147.
[34] J.J. Wu, S.C. Liu, Catalyst-free growth and characterization of ZnO nanorods, J. Phys. Chem. B 106 (2002) 9546–9551.
[35] H.B. Fu, T.G. Xu, S.B. Zhu, Y.F. Zhu, Photocorrosion Inhibition and;1; Enhancement of Photocatalytic Activity for ZnO via Hybridization with C-60, Environ. Sci. Technol. 42 (2008) 8064–8069.
[36] N. Kislov, J. Lahiri, H. Verma, D.Y. Goswami, E. Stefanakos, M. Batzill, Photocatalytic degradation of methyl orange over single crystalline ZnO: orientation dependence of photoactivity and photostability of ZnO, Langmuir 25 (2009) 3310–3315.
[37] Y.Y. Wen, H.M. Ding, Y.K. Shan, Preparation and visible light photocatalytic activity of Ag/TiO2/graphene nanocomposite, Nanoscale 3 (2011) 4411–4417.
[38] J.X. Low, J.G. Yu, Q. Li, B. Cheng, Enhanced visible-light photocatalytic activity of plasmonic Ag and graphene co-modified Bi2WO6 nanosheets, Phys. Chem. Chem. Phys. 16 (2014) 1111–1120.
[39] W.H. Leng, Z. Zhang, J.Q. Zhang, C.N. Cao, Investigation of the kinetics of a TiO2 photoelectrocatalytic reaction involving charge transfer and recombination through surface states by electrochemical impedance spectroscopy, J. Phys. Chem. B 109 (2005) 15008–15023.
[40] J.M. Herrmann, H. Tahiri, Y. AitIchou, G. Lassaletta, A.R. GonzalezElipe, A. Fernandez, Characterization and photocatalytic activity in aqueous medium of TiO_2 and Ag-TiO_2 coatings on quartz, Appl. Catal. B: Environ. 13 (1997) 219–228.
[41] H.M. Sung-Suh, J.R. Choi, H.J. Hah, S.M. Koo, Y.C. Bae, Comparison of Ag deposition effects on the photocatalytic activity of nanoparticulate TiO_2 under visible and UV light irradiation, J. Photochem. Photobiol. A: Chem. 163 (2004) 37–44.
[42] H.Y. Chuang, D.H., Chen, Fabrication and photocatalytic activities in visible and UV light regions of Ag@TiO2 and NiAg@TiO2 nanoparticles, Nanotechnology, 20 (2009) -.
[43] G. Zhao, H. Kozuka, T. Yoko, Sol-gel preparation and photoelectrochemical properties of TiO_2 films containing Au and Ag metal particles, Thin Solid Films 277 (1996) 147–154.
[44] T.X. Wu, G.M. Liu, J.C. Zhao, H. Hidaka, N. Serpone, Photoassisted degradation of dye pollutants. V. Self-photosensitized oxidative transformation of Rhodamine B under visible light irradiation in aqueous TiO_2 dispersions, J. Phys. Chem. B 102 (1998) 5845–5851.